Available online at www.sciencedirect.com
SCIENCE DIRECT®
Journal of Computational Physics 197 (2004) 341–363
JOURNAL OF COMPUTATIONAL PHYSICS
www.elsevier.com/locate/jcp

Efficient fast multipole method for low-frequency scattering

Eric Darve [a,b,*], Pascal Havé [c]

[a] Mechanics and Computation division, 262 Durand building, Room 265 Stanford, CA 94305-4040, USA
[b] Mechanical Engineering Department, Stanford University, Stanford, CA, USA
[c] Université Pierre et Marie Curie, Jacques-Louis Lions laboratory, France

Received 24 May 2001; received in revised form 19 November 2003; accepted 2 December 2003
Available online 22 January 2004

Abstract

The solution of the Helmholtz and Maxwell equations using integral formulations requires to solve large complex linear systems. A direct solution of those problems using a Gauss elimination is practical only for very small systems with few unknowns. The use of an iterative method such as GMRES can reduce the computational expense. Most of the expense is then computing large complex matrix vector products. The cost can be further reduced by using the fast multipole method which accelerates the matrix vector product. For a linear system of size N, the use of an iterative method combined with the fast multipole method reduces the total expense of the computation to $N \log N$. There exist two versions of the fast multipole method: one which is based on a multipole expansion of the interaction kernel $\exp \imath kr/r$ and which was first proposed by V. Rokhlin and another based on a plane wave expansion of the kernel, first proposed by W.C. Chew. In this paper, we propose a third approach, the stable plane wave expansion (SPW-FMM), which has a lower computational expense than the multipole expansion and does not have the accuracy and stability problems of the plane wave expansion. The computational complexity is $N \log N$ as with the other methods.

AMS: 31B10; 33C10; 41A58; 42B10; 65R20; 65T20; 65Y20; 70F10; 78A45

Keywords: Fast multipole method; Laplace; Maxwell; Helmholtz; Electromagnetic scattering; Low-frequency scattering; Plane wave; Evanescent wave

1. Background and motivation

1.1. Multipole expansion

The basic problem [1] that the fast multipole method is addressing is the one of computing large matrix vector products, where the matrix is defined by

* Corresponding author. Tel.: +1-650-725-2560; fax: +1-650-723-1778.
E-mail addresses: darve@stanford.edu (E. Darve), have@ann.jussieu.fr (P. Havé).
URL: http://me.stanford.edu/faculty/facultydir/darve.html.

0021-9991/$ - see front matter
doi:10.1016/j.jcp.2003.12.002

$$M_{ij} = \frac{\exp \imath\kappa|r_i - r_j|}{|r_i - r_j|}.$$

The fast multipole method of Rokhlin–Greengard [2–4] is based on the following multipole expansion:

$$h_0^{(1)}(r + r') = \sum_{n=0}^{+\infty} (-1)^n (2n+1) h_n^{(1)}(\kappa|r|) j_n(\kappa|r'|) P_n(r \cdot r'), \tag{1}$$

where $h_n^{(1)}$ is the spherical Hankel function, j_n the spherical Bessel function and P_n the Legendre polynomial. As the fast multipole method has been described in more detail elsewhere [4–7], we will only summarize the key formulas here so that the notations are clarified. Two fundamental solutions can be defined, one which is regular, the other singular at $r = 0$:

$$I_n^m(r) = \imath^n j_n(\kappa|r|) L_n^m(\theta, \phi),$$
$$O_n^m(r) = \imath^n h_n^{(1)}(\kappa|r|) N_n^m(\theta, \phi),$$

where L_n^m and N_n^m are equal to spherical harmonics up to the choice of normalizing constants:

$$L_n^m(\theta, \phi) = \frac{\sqrt{2n+1}}{(n+|m|)!} P_n^m(\cos\theta)\, \mathrm{e}^{-\imath m\phi},$$
$$N_n^m(\theta, \phi) = \sqrt{2n+1}(n-|m|)! P_n^m(\cos\theta)\, \mathrm{e}^{\imath m\phi}.$$

P_n^m are the Associated Legendre functions.

With these choices, the formula are somewhat simplified. Eq. (1) becomes

$$h_0^{(1)}(r + r') = \sum_{n=0}^{+\infty} \sum_{m=-n,\ldots,n} I_n^m(r) O_n^m(r').$$

The usual transforms (Inner-to-Inner, Outer-to-Outer and Inner-to-Outer) are defined in terms of the function E, which is related to the Wigner $3-j$ symbols [4],

$$E\begin{pmatrix} m & p & r \\ n & q & s \end{pmatrix} = \frac{1}{4\pi} \int\int N_n^m(\theta, \phi) N_q^p(\theta, \phi) L_s^r(\theta, \phi) \sin\theta \,\mathrm{d}\theta \,\mathrm{d}\phi.$$

The Inner-to-Outer transform then reads

$$O_n^m(r + r') = \sum_{m,n,m',n',s} E\begin{pmatrix} mm' & m+m' \\ nn' & n+n'-2s \end{pmatrix} I_{n'(r)}^{m'} O_{n+n'-2s}^{m+m'}(r').$$

Similar equations hold for the Outer-to-Outer and Inner-to-Inner transforms.

This approach has two disadvantages which our technique addresses. First, it is not applicable to the high-frequency regime. In fact it can be shown that the number of terms needed in the multipole expansion (number of terms in Eq. (1), for example) is on the order of κD, where D is the diameter of the object. As κD becomes large the method becomes very costly. In the high-frequency regime it is very common that hundreds of terms are needed to start observing a convergence of Eq. (1). Therefore, it is impractical.

Second, the cost of applying the method in the low-frequency regime is still quite high. In fact, the computation of the function E and its multiplication by $O_{n+n'-2s}^{m+m'}(r')$ requires a total of $\mathrm{O}(p^5)$ flops (floating point operations) for an order p expansion.

Several improvements were made to this original approach. Among the many publications, for the Laplace equation, we can cite [8], where Elliott and Board reduced the algorithmic complexity by using the fast Fourier transforms and a block decomposition to improve stability and efficiency. Greengard and Rokhlin [9] introduced two improvements: one is based on rotation matrices (see [10] for a similar method) and one uses a plane wave expansion, which provides a diagonal multipole-to-local operator. Zhao and Chew applied a matrix rotation scheme to reduce the storage requirement, see [11]. For the Helmholtz equation, Greengard et al. in [12] proposed a variant of the scheme described in this paper to speed up the multipole-to-local operation.

Note that in order to make this method stable at very low frequencies, a renormalization of the coefficients is required. Indeed, due to asymptotic behaviors of j_n ($j_n(x) \to 0$, when $x \to 0$) and $h_n^{(1)}$ ($h_n^{(1)}(x) \to \infty$, when $x \to 0$), numerical instabilities may occur at very low frequency. This procedure is described in [13,14]. See [15] for an application of LF-MLFMA to low-frequency problems.

For LF-MLFMA (low-frequency regime), the cost of the multipole-to-local operation requires $O(p^4)$ flops, where p denotes the truncation parameter in Eq. (1). We will show that our new expansion, stable plane wave FMM (SPW-FMM), reduces the cost of the multipole-to-local operation to $O(p^2)$ flops and therefore is competitive with previously published schemes.

1.2. Plane wave expansion

To address the problem of an increase number of multipole terms in the high-frequency regime [16–21], a different approach was taken based on an approximation of the form:

$$\frac{e^{\imath\kappa|r+r'|}}{|r+r'|} = \lim_{p\to+\infty} \int_{S^2} e^{\imath\kappa\langle\sigma,r'\rangle} T_{p,\sigma}(r)\,d\sigma, \tag{2}$$

where S^2 is the unit sphere. We denote by $\langle\cdot,\cdot\rangle$ the scalar product. The function $T_{p,\sigma}(r)$ is defined by

$$T_{p,\sigma}(r) = \imath\kappa \sum_{m=0}^{p} \frac{(2m+1)\imath^m}{4\pi} h_m^{(1)}(\kappa|r|) P_m(\cos(\sigma,r)). \tag{3}$$

The integral is then discretized and an appropriate integer p is chosen so that

$$\frac{e^{\imath\kappa|r+r'|}}{|r+r'|} \approx \sum_k \omega_k\, e^{\imath\kappa\langle\sigma_k,r'\rangle} T_{p,\sigma}(r). \tag{4}$$

Several publications have studied how to appropriately choose the discretization points and the order p for a given accuracy ϵ.

With this approach the cost on the Inner-to-Outer transform is reduced to $O(p^2)$. This guarantees a computational expense on the order of $N \log N$ in the high-frequency regime.

This method has proved to be very successful. For example, W.C. Chew has made impressive radar computations using this approach (see [18,19,22–30]). However, the method has some drawbacks and is unstable at low-frequency or high order. The transfer function $T_{p,\sigma}(r)$ is defined in terms of $h_m^{(1)}(\kappa|r|)$ which have the property of diverging when $m \to +\infty$ (high order) or $\kappa|r| \to 0$ (low frequency). Our approach, SPW-FMM, solves this problem by being stable in the high and low-frequency regime, and being arbitrarily accurate numerically. The total asymptotic cost is $O(N \log N)$ as for the other methods and the Inner-to-Outer transform is performed in $O(p^2)$ flops.

1.3. Note on accuracy

There has been some debate regarding the accuracy of Eq. (4). It has been proved in several publications that the error in the method is controllable. See, for example, [20,31–36]. However, when the method is implemented numerically the roundoff errors make it unstable. This imposes a lower bound on the error.

In [37], Ohnuki and Chew reviews the various sources of error and demonstrates that the error is controllable. The footnote on page 774 in [37] mentions that "this paper is motivated by a reviewer's comment on one of our papers that MLFMA is not error controllable." However, the analysis in [37] does not take into account roundoff errors. As the order becomes larger, the transfer function diverges and roundoff errors ultimately corrupt the solution. To illustrate this fact, we computed $H_0^{(1)}(\kappa\rho_{ji})$ using two different equations (the notations are from [37]):

Approximation 1:

$$\sum_{m=-P}^{P} J_m(\kappa\rho_{jl'})\,\mathrm{e}^{\imath m(\phi_{jl'}-\pi)} \sum_{n=\max(-P,m-P)}^{\min(P,m+P)} H_{m-n}^{(1)}(\kappa\rho_{l'l})\,\mathrm{e}^{-\imath(m-n)\phi_{l'l}}\,J_n(\kappa\rho_{li})\,\mathrm{e}^{-\imath n\phi_{li}}. \tag{5}$$

Approximation 2:

$$\frac{1}{Q}\sum_{q=1}^{Q} \mathrm{e}^{-\imath\kappa\rho_{jl'}\cos(\alpha_q-\phi_{jl'})}\left[\sum_{p=-P}^{P} H_p^{(1)}(\kappa\rho_{l'l})\,\mathrm{e}^{-\imath p(\phi_{l'l}-\alpha_q+\frac{\pi}{2})}\right]\mathrm{e}^{-\imath\kappa\rho_{li}\cos(\alpha_q-\phi_{li})}. \tag{6}$$

Approximation 1 is the standard multipole expansion, whereas approximation 2 is the plane wave expansion. The instability comes from $H_p^{(1)}(\kappa\rho_{l'l})$ which diverges as $p\to+\infty$. These two approximations are equally accurate for a given P except when roundoff errors start contaminating the solution. For large P, approximation 1 remains stable (a renormalization is needed), whereas approximation 2 is unstable (this cannot be corrected).

The points $\boldsymbol{\rho}_l$, $\boldsymbol{\rho}_i$, $\boldsymbol{\rho}_{l'}$ and $\boldsymbol{\rho}_j$ are defined in terms of a parameter d which controls the distance between those points (effectively whether we are in a low- or high-frequency regime):

$$\boldsymbol{\rho}_l=\begin{pmatrix}0\\0\end{pmatrix},\quad \boldsymbol{\rho}_i=\begin{pmatrix}-d/\sqrt{8}\\-d/\sqrt{8}\end{pmatrix},\quad \boldsymbol{\rho}_{l'}=\begin{pmatrix}2d\\0\end{pmatrix},\quad \boldsymbol{\rho}_j=\begin{pmatrix}2d+d/\sqrt{8}\\d/\sqrt{8}\end{pmatrix}.$$

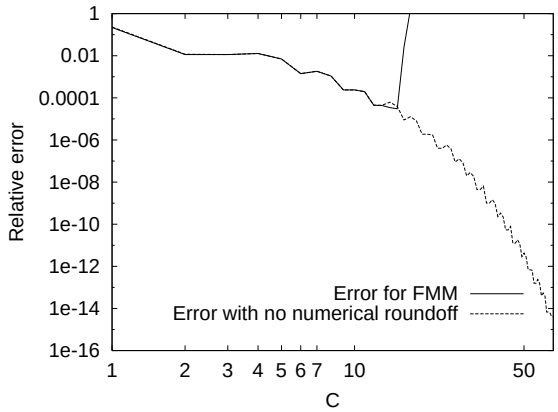

Fig. 1. Error due to roundoff and numerical instability. The error for the FMM is obtained using Approximation 2 and the error without roundoff errors is obtained using Approximation 1.

In our calculations shown in Fig. 1, we chose $\kappa = 1$, $d = 5/2$. The parameter Q was chosen large enough to capture the whole bandwidth of the signal. The integer P was chosen equal to $P = \kappa d + C(\kappa d)^{1/3}$ for different choices of C (see [37, p. 775 and 777]).

2. Stable plane wave expansion – SPW-FMM

The proposed method is based on the following approximation which resembles Eq. (4):

$$\frac{e^{\imath\kappa|r|}}{|r|} = \frac{\imath\kappa}{2\pi}\int_{S^{z+}} e^{\imath\kappa\langle\sigma,r\rangle}\,d\sigma + \frac{1}{\pi}\int_{\chi=0}^{+\infty}\int_{\phi=0}^{2\pi} e^{-\chi^2 z}\, e^{\imath\sqrt{\chi^4+\kappa^2}(x\cos\phi+y\sin\phi)}\,\chi\,d\chi\,d\phi, \tag{7}$$

with $r = (x, y, z)$ and S^{z+} is the subset of the unit sphere of all points with positive z-coordinate (upper hemisphere). This formula was first proposed by Greengard et al. [12]. Even though our approach is based on the same integral, it is, as we will see, different. In particular it uses a single expansion, the stable plane wave expansion, rather than a combination of plane wave expansion and classical multipole expansion. New interpolation and anterpolation algorithms are constructed to go from a fine level to a coarser level and vice versa. These algorithms are not found in [12] since these operations are taken care of by the classical operators for multipole and local expansions. Therefore, the methods are truly different. Compared to [12], the new expansions have the advantage of being applicable at all frequencies, whereas in the high-frequency regime, [12] becomes costly, in particular, the conversion from multipole expansion to plane wave expansion and vice versa, and the shift of the origin of the expansions.

A technique, based on an integral similar to Eq. (7) has been proposed by Hu et al. The scheme is called FIPWA. This work is described in several publications [38–43]. The difference between FIPWA and Eq. (7) is that the path of the integral in the complex plane is different. FIPWA uses the steepest descent path, whereas for Eq. (7) the path is parallel to the real or the imaginary axis (see [43], for example).

2.1. Quadrature

We now discuss the choice of quadrature points. We denote by $\omega_k^\sigma, \sigma_k$ and $\omega_k^{\chi\phi}, \chi_k, \phi_k$ the quadrature weights and points. For two vectors r and r', denoting $r' = (x', y', z')$, we then use the following approximation:

$$\frac{e^{\imath\kappa|r+r'|}}{|r+r'|} \approx \frac{\imath\kappa}{2\pi}\sum_k \omega_k^\sigma(r)\, e^{\imath\kappa\langle\sigma_k,r'\rangle} + \frac{1}{\pi}\sum_k \chi_k(r)\, e^{-\chi_k^2 z'}\, e^{\imath\sqrt{\chi_k^4+\kappa^2}(x'\cos\phi_k+y'\sin\phi_k)}. \tag{8}$$

To clarify the role of r and r', let us take an example. Assume we have two points r_i and r_j in clusters C_a and C_b of center O_a and O_b. Then

$$r = O_a - O_b,$$
$$r' = (r_i - O_a) - (r_j - O_b).$$

In general, with a cubic oct-tree decomposition,

$$|r| > \frac{2}{\sqrt{3}}|r'|.$$

For this expansion to be practical we need to satisfy the following condition:

Condition 1. There must exist a constant C such that: For all r and r' for which Eq. (8) is used, we have:

$$z > 0 \quad \text{and} \quad \sqrt{x^2 + y^2} < Cz,$$

where $r + r' = (x, y, z)$.

When this condition is satisfied, the second integral is bounded and the number of discretization points needed for ϕ, n_ϕ remains small. In general, the larger C is, the larger n_ϕ is. In a standard 3D oct-tree decomposition, if we consider two clusters in the interaction list (see paper by Greengard for definition of the interaction list), we can always choose x, y and z so that

$$z > 0 \quad \text{and} \quad \sqrt{x^2 + y^2} < 3\sqrt{2}z.$$

Therefore, this condition is naturally met. Regarding the number of discretization point needed for ϕ, we can prove the following result.

Proposition 1. *Assume that $z \ll 1/\kappa$, then the number of discretization points for ϕ, n_ϕ, is independent of the size of the cluster and is a function of the tolerance ϵ only.*

Assume that $z \gg 1/\kappa$, then the number of discretization points for ϕ is a function of the size of the cluster and of the tolerance ϵ. In general: $n_\phi \approx \kappa\sqrt{x^2 + y^2}$.

In both cases, we can choose quadrature points ϕ_k which are uniformly distributed between 0 and 2π.

The analysis for the case $z \gg 1/\kappa$ is actually identical to the analysis for the standard plane expansion of Eq. (4). It says that the number of quadrature points is not just a function of ϵ but a function of the size of the cluster also.

Proof. Use the following two results:

$$e^{\imath\kappa\langle\sigma,r\rangle} = \sum_{p=0}^{\infty} (2p+1)\imath^p j_p(\kappa|r|) P_p(\cos(\sigma, r)), \tag{9}$$

where $\cos(\sigma, r)$ is the cosine of the angle between σ and r, and

$$j_p(\kappa|r|) \sim \frac{1}{2p+1}\sqrt{\frac{e}{2}}\left(\frac{e\kappa|r|}{2p+1}\right)^p \quad \text{for } p \to +\infty. \qquad \square \tag{10}$$

The number of discretization points for χ is more complicated to derive. However, we will show that it is independent of the size of the cluster and is a function of ϵ only.

The analysis for σ is the following. We are approximating the integral:

$$\int_{S^{z+}} e^{\imath\kappa\langle\sigma,r+r'\rangle}\, d\sigma = \int_{S^{z+}} e^{\imath\kappa\langle\sigma,r+r'\rangle} \sin\theta\, d\theta\, d\psi.$$

Proposition 2. *The number of discretization points for ψ, n_ψ, is a function of ϵ and r' and is on the order of $\kappa|r'|$. The points ψ_k can be chosen uniformly distributed between 0 and 2π.*

An upper bound for n_ψ can be found numerically by looking at the bandwidth in Fourier space of $e^{\imath\kappa|r'|\cos\psi}$.

Proof. Use Eqs. (9) and (10) to establish that the bandwidth of $e^{\imath\kappa\langle\sigma,r'\rangle}$ for ψ is on the order of $\kappa|r'|$ and is smaller than the bandwidth of $e^{\imath\kappa|r'|\cos\psi}$, which we denote $n_\psi^{\max}$. By convention, we define the bandwidth of a function as twice its largest frequency in Fourier space.

Any frequency for $e^{\imath\kappa\langle\sigma,r\rangle}$ for variable ψ which is larger than $n_\psi^{\max}/2$ does not contribute to the integral. After smoothing the function $e^{\imath\kappa\langle\sigma,r\rangle}$ by removing frequencies in ψ larger than $n_\psi^{\max}/2$, we can choose quadrature points for ψ uniformly distributed between 0 and 2π. We need no more than $n_\psi^{\max}$ points.

Note that in some cases r can be as large as: $|r| > 3\max_{ij}|r'|$. Therefore, $e^{\imath\kappa\langle\sigma,r\rangle}$ will have frequencies significantly larger than $n_\psi^{\max}/2$. □

The same strategy can be applied to ϕ and allows to reduce n_ϕ so that in general n_ϕ can be chosen equal to $n_\phi^{\max}$, where $n_\phi^{\max}$ is the bandwidth of $\exp(\imath\sqrt{\chi_k^4+\kappa^2}\sqrt{(x')^2+(y')^2}\cos\phi)$. In particular, in the case $z \gg 1/\kappa$, we can choose $n_\phi^{\max} \approx \kappa\sqrt{(x')^2+(y')^2}$. Without the algorithm described in the proof of Proposition 2, the estimate is $n_\phi^{\max} \approx \kappa\sqrt{x^2+y^2}$ (Proposition 1), which can be much larger.

We now turn to θ:

$$\int_{S^{z+}} e^{\imath\kappa\langle\sigma,r+r'\rangle}\,d\sigma = \int_0^{2\pi} d\theta \int_0^{2\pi} d\psi \mathbf{1}_{[0:\pi/2]}(\theta)\sin\theta\, e^{\imath\kappa\langle\sigma,r\rangle}\, e^{\imath\kappa\langle\sigma,r'\rangle},$$

where

$$\mathbf{1}_{[0:\pi/2]}(\theta) = \begin{cases} 1 & \text{if } \theta \in [0:\pi/2], \\ 0, & \text{otherwise.} \end{cases}$$

The first difficulty to integrate this function is that it is not possible to simply use a uniform distribution of points for the integration along θ. The reason is that as the function is discontinuous its Fourier spectrum decays slowly.

Let us introduce the following notation:

$$S(\theta,\psi) = (2\pi-\theta, \pi+\psi).$$

As

$$\sigma(S(\theta,\psi)) = \sigma(\theta,\psi),$$

we can write

$$\int_{S^{z+}} e^{\imath\kappa\langle\sigma,r+r'\rangle}\,d\sigma = \int_0^{2\pi} d\theta \int_0^{2\pi} d\psi \frac{1}{2}\left(\mathbf{1}_{[0:\pi/2]}(\theta)\sin\theta + \mathbf{1}_{[0:\pi/2]}(2\pi-\theta)\sin(2\pi-\theta)\right) e^{\imath\kappa\langle\sigma,r+r'\rangle}.$$

To simplify the notations, we introduce

$$F^\sigma(\theta,\psi) = \frac{1}{2}\left(\mathbf{1}_{[0:\pi/2]}(\theta)\sin\theta + \mathbf{1}_{[0:\pi/2]}(2\pi-\theta)\sin(2\pi-\theta)\right) e^{\imath\kappa\langle\sigma,r\rangle}.$$

The following proposition will now be proved.

Proposition 3. *The number of discretization points for θ, n_θ, is a function of ϵ and r' and is on the order of $\kappa|r'|$. The points θ_k can be chosen uniformly distributed between 0 and 2π.*

An upper bound for n_θ can be found numerically by looking at the bandwidth in Fourier space of $e^{\imath\kappa|r'|\cos\theta}$.

Proof. Using Eqs. (9) and (10), the bandwidth of $e^{\imath\kappa\langle\sigma,r'\rangle}$ for θ is of the order of $\kappa|r'|$ and is smaller than the bandwidth of $e^{\imath\kappa|r'|\cos\theta}$, $n_\theta^{\max}$.

The key point is that any frequency for $F^\sigma(\theta,\psi)$ for variable θ which is larger than $n_\theta^{\max}/2$ does not contribute to the integral. This is the same argument as before. After removing all the frequencies of

$F^\sigma(\theta,\psi)$ larger than $n_\psi^{\max}/2$, we can choose $n_\psi^{\max}$ quadrature points for ψ uniformly distributed between 0 and 2π. □

Note that the storage and computational expense can be reduced by a factor of 2 by noticing that:

$$e^{\imath\kappa\langle\sigma(\theta,\psi),r\rangle} = e^{\imath\kappa\langle\sigma(S(\theta,\psi)),r\rangle},$$
$$F^\sigma(\theta,\psi) = F^\sigma(S(\theta,\psi)).$$

Therefore, we only need to store and compute angles θ such that $0 \leqslant \theta \leqslant \pi$.

3. Gathering and scattering steps

Special care must be taken when gathering information from children to the parent or scattering information from the parent to the children. This issue is very similar to the situation described in the standard plane wave expansion method. We will refer the reader to previously published articles to get the details [20–25]. To summarize the issue, we simply state that when gathering we need to increase the number of sample points to reflect a larger bandwidth in Fourier space. On the contrary, when scattering we can downsample to reflect a decrease in bandwidth.

Considering the functions

$$e^{\imath\kappa\langle\sigma(\theta,\psi),r'\rangle},$$

$$e^{-\chi^2 z'}\, e^{\imath\sqrt{\chi^4+\kappa^2}(x'\cos\phi + y'\sin\phi)}$$

and the discussion in Section 2, the standard algorithm can be applied to variables θ, ψ and ϕ. Fast Fourier transforms can be used to oversample and downsample very efficiently. A similar method is described in [21].

Care must be taken for variable χ. It looks like the function

$$G^{z\rho}(\chi) = e^{-\chi^2 z}\, e^{\imath\sqrt{\chi^4+\kappa^2}\rho}$$

should have a Fourier spectrum similar to

$$e^{-\chi^2 z}\, e^{\imath\kappa\rho},$$

for large z and ρ. The author was not able to find an elegant proof of this fact. The general argument is that for large z, χ has to be small otherwise $e^{-\chi^2 z}$ becomes negligible. Therefore,

$$z \gg \frac{1}{\kappa} \;\Rightarrow\; \left\{ \left| e^{-\chi^2 z}\, e^{\imath\sqrt{\chi^4+\kappa^2}\rho} \right| \leqslant \epsilon \text{ or } \chi^2 \ll \kappa. \right.$$

On the contrary for $z \ll (1/\kappa)$, $G^{z\rho}(\chi)$ should have a Fourier spectrum similar to

$$e^{-\chi^2 z}\, e^{\imath\chi\rho}.$$

In both cases, the expected behavior is that the spectrum should be similar to a Gaussian. In the intermediate region, where $z \approx 1/\kappa$, the behavior is less clear.

In the absence of a rigorous mathematical study, the author resorted to numerical tests.

The first plot (Fig. 2) is the Fourier spectrum of $G^{z\rho}(\chi)$ for various z, $\rho = z$ and $\kappa = 1$. Obviously the choice of $\kappa = 1$ is general since the coordinates can be scaled so that $\kappa = 1$. The spectrum is compared with

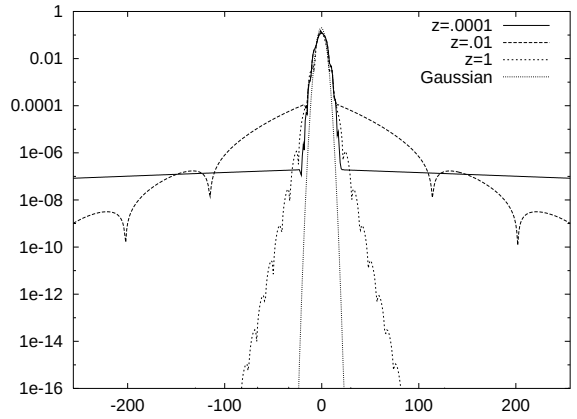

Fig. 2. Fourier spectrum of $G^{z\rho}(\chi)$ in the low-frequency regime.

a Gaussian. It clearly shows that in the mid-range $z = 10^{-2}$, the Fourier spectrum decays very slowly. However, in the very low-frequency regime $z = 0.0001\kappa$, there is a fast decay followed by a plateau around 10^{-7}. As we reduce z, the behavior is similar with a fast decay followed by a plateau which we found empirically to be around $10^{-3}z$.

The second plot (Fig. 3) is similar but corresponds to the high-frequency regime. The spectrum is very close to a Gaussian and the decay increases with z.

These two plots confirmed the sketched analysis. The conclusion is that:

- In the very low-frequency regime ($z \lesssim 10^{-4}/\kappa$) and in the high-frequency regime ($z \gtrsim 1/\kappa$), the spectrum decays rapidly like a Gaussian.
- In the low-frequency regime ($z \approx 10^{-2}/\kappa$), the decay is very slow.

We now ask the following question. For a given error ϵ, how many uniformly distributed quadrature points χ do we need to represent $G^{z\rho}(\chi)$? We selected $\epsilon = 10^{-6}$ and plotted (Fig. 4) the number of quadrature points needed as a function of z. In the very low-frequency regime ($z < 10^{-4}/\kappa$) and in the high-frequency regime ($z > 1/\kappa$), the spectrum is similar to a Gaussian and, therefore, decays very fast. This results in very

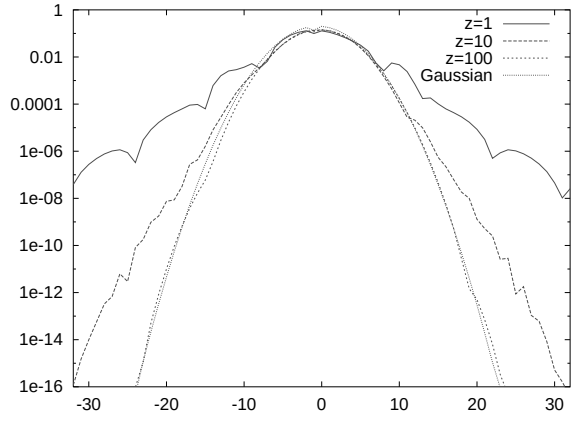

Fig. 3. Fourier spectrum of $G^{z\rho}(\chi)$ in the high-frequency regime.

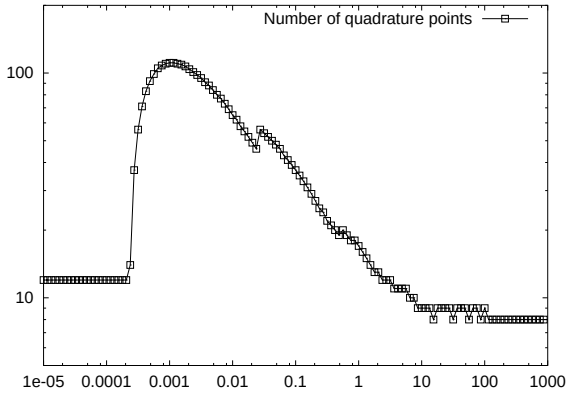

Fig. 4. Number of uniformly distributed quadrature points χ as a function of z.

few quadrature points. In the intermediate region ($z \approx 10^{-2}/\kappa$), many points are required to represent $G^{z\rho}(\chi)$.

The practical implication of these observations is that a standard smoothing and interpolating strategy based on Fourier transforms [20,21] is applicable in the very low and high-frequency regime. In the intermediate regime another approach must be taken. It is based on an SVD decomposition.

4. SVD decomposition

The method is based on the SVD of:

$$K(\chi, z, \rho) \stackrel{\text{def}}{=} \exp(-\chi z)\exp(\imath\rho\sqrt{\chi^2+\kappa^2}).$$

For a multilevel method, we need a different SVD at each level. At level l, we choose (χ, z, ρ) in the following intervals:

$$\chi \in [0 : \chi_{\max}]\exp(-\chi_{\max}2^l) \leqslant \epsilon,$$
$$z \in [2^l : 2^{l+1}],$$
$$\rho \in [-2^l/\sqrt{2} : 2^l/\sqrt{2}].$$

For simplicity, we assume from now on that the finest clusters have length 1 and the finest level corresponds to $l = 0$. The SVD is the following decomposition of $K(\chi, z, \rho)$:

$$K(\chi, z, \rho) = \sum_{p=0}^{+\infty} s_p^l u_p^l(\chi) v_p^l(z, \rho),$$

where s_p^l are all positive numbers, u_p^l and v_p^l are two sets of orthonormal complex functions.

In our case, we use an approximate decomposition, where for an integer n^l we have

$$\left| K(\chi, z, \rho) - \sum_{p=0}^{n^l} s_p^l u_p^l(\chi) v_p^l(z, \rho) \right| \leqslant \epsilon,$$

for all (χ, z, ρ) in the appropriate intervals.

For more details on this decomposition and how to compute it numerically see [44].

Numerical tests show that a small number of coefficients is needed to efficiently approximate $K(\chi, z, \rho)$. For example, for $z = 10^{-3}$, we computed the number of quadrature points p as function of the error ϵ. We can observe (Fig. 5) that p is $O(\log \epsilon)$.

In the low-frequency regime, the largest number of quadrature points given by SVD for $\epsilon = 10^{-6}$ is 10 (Fig. 6), which is much better than before (see Fig. 4 with a maximum above 100). Moreover, for very low-frequency and high-frequency regimes, the quadrature is always smaller than with uniformly distributed points.

To take advantage of the SVD decomposition, we compute the following variables, for each cluster C_a^l at level l:

$$\lambda_p^{a,l}(\phi) = \int_0^{\chi_{\max}} (u_p^l(\chi))^* \left(\sum_i J_i K(\chi, z_i - z_\lambda^{a,l}, (x_i - x_\lambda^{a,l}) \cos\phi + (y_i - y_\lambda^{a,l}) \sin\phi) \right) \mathrm{d}\chi.$$

The sum is over all sources located at (x_i, y_i, z_i) in cluster C_a^l, and of intensity J_i. We denote O_a^l the center of C_a^l and r^l the length of the side of the cluster. With these notations, the reference center $(x_\lambda^{a,l}, y_\lambda^{a,l}, z_\lambda^{a,l})$ must be located at the following point:

$$\begin{cases} x_\lambda^{a,l} = x_{O_a^l}, \\ y_\lambda^{a,l} = y_{O_a^l}, \\ z_\lambda^{a,l} = z_{O_a^l} + \frac{3}{2} r^l. \end{cases}$$

Proposition 4. *The choice of $(x_\lambda^{a,l}, y_\lambda^{a,l}, z_\lambda^{a,l})$ is optimal in the sense that for a given error ϵ, we have a minimal number of terms in the SVD decomposition.*

Proof. Let us introduce a parameter α and choose the reference center at:

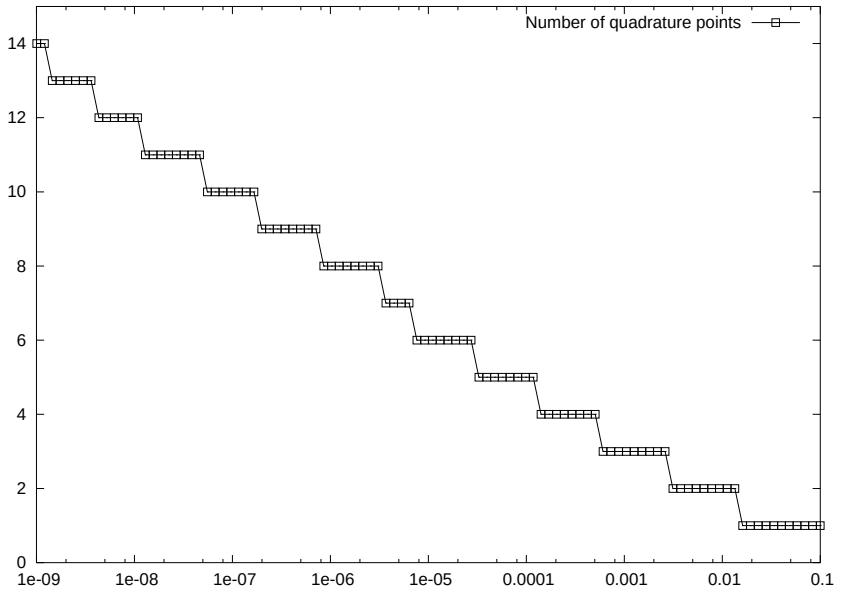

Fig. 5. Number of quadrature points χ as function of ϵ, given by SVD.

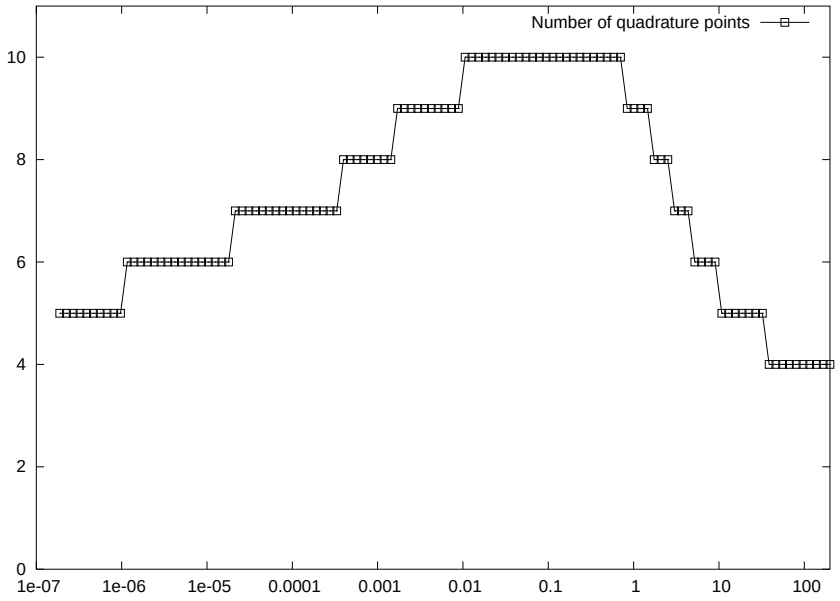

Fig. 6. Number of quadrature points χ as function of z, given by SVD.

$$\begin{cases} x_\lambda^{a,l} = x_{O_a^l}, \\ y_\lambda^{a,l} = y_{O_a^l}, \\ z_\lambda^{a,l} = z_{O_a^l} + (\alpha + \frac{1}{2})r^l. \end{cases}$$

Then, the SVD decomposition must be computed for:

$$\chi \in [0 : \chi_{\max}] \exp(-\chi_{\max}\alpha) \leqslant \epsilon,$$
$$z \in [\alpha : 1 + \alpha],$$
$$\rho \in [-2^l/\sqrt{2} : 2^l/\sqrt{2}]$$

at level 0, for example. When α is small $\chi_{\max}$ is large and therefore, K becomes very oscillatory in ρ, which means that the SVD decomposition will converge slower.

On the other hand, when $\alpha > 1$, the function:

$$\sum_i J_i K(\chi, z_i - z_\lambda^{a,l}, (x_i - x_\lambda^{a,l})\cos\phi + (y_i - y_\lambda^{a,l})\sin\phi)$$

must be multiplied by

$$K(\chi, z_\lambda^{a,l} - z_j, (x_\lambda^{a,l} - x_j)\cos\phi + (y_\lambda^{a,l} - y_j)\sin\phi).$$

In general, $z_\lambda^{a,l} - z_j$ can be negative unless $\alpha \leqslant 1$. If $z_\lambda^{a,l} - z_j$ is negative, the function $K(\chi, z_\lambda^{a,l} - z_j, \ldots)$ can be arbitrarily large and therefore, the method is unstable.

The optimal value is therefore $\alpha = 1$. □

We now introduce the following matrix:

$$M_{pq}^{l}(z, x\cos\phi + y\sin\phi) = \int (u_p^{l+1}(\chi))^* K(\chi, z, x\cos\phi + y\sin\phi) u_q^l(\chi)\,\mathrm{d}\chi.$$

Proposition 5. *Assume that cluster C_b^{l+1} is the parent of cluster C_a^l. Then,*

$$\left| \lambda_p^{b,l+1}(\phi) - \sum_{q=1}^{n^l} M_{pq}^l(z, x\cos\phi + y\sin\phi)\lambda_q^{a,l}(\phi) \right| \leqslant \epsilon,$$

where

$$\begin{cases} x = x_\lambda^{a,l} - x_\lambda^{b,l+1}, \\ y = y_\lambda^{a,l} - y_\lambda^{b,l+1}, \\ z = z_\lambda^{a,l} - z_\lambda^{b,l+1}. \end{cases}$$

Proof. Use the SVD decomposition of K,

$$K(\chi, z, \rho) \approx \sum_{p=0}^{n^l} s_p^l u_p^l(\chi) v_p^l(z, \rho),$$

and the fact that $u_p^{l+1}(\chi)$ is an orthonormal basis. □

The scattering phase is done in the same manner, albeit with the transpose of M_{pq}. We introduce the following coefficients:

$$\mu_p^{a,l}(\phi) = \int_0^{\chi_{\max}} u_p^l(\chi) \left(\sum_i J_i K(\chi, z_i - z_\mu^{a,l}, (x_i - x_\mu^{a,l})\cos\phi + (y_i - y_\mu^{a,l})\sin\phi) \right) \mathrm{d}\chi$$

for all sources i far away from cluster C_a^l, where now

$$\begin{cases} x_\mu^{a,l} = x_{O_a^l}, \\ y_\mu^{a,l} = y_{O_a^l}, \\ z_\mu^{a,l} = z_{O_a^l} - \frac{3}{2} r^l. \end{cases}$$

The following proposition is true:

Proposition 6. *Assume that cluster C_b^{l+1} is the parent of cluster C_a^l. Then*

$$\left| \mu_p^{a,l}(\phi) - \sum_{q=1}^{n^{l+1}} M_{qp}^l(z, x\cos\phi + y\sin\phi)\mu_q^{b,l+1}(\phi) \right| \leqslant \frac{\epsilon}{s_p^l}, \tag{11}$$

where

$$\begin{cases} x = x_\mu^{b,l+1} - x_\mu^{a,l}, \\ y = y_\mu^{b,l+1} - y_\mu^{a,l}, \\ z = z_\mu^{b,l+1} - z_\mu^{a,l}. \end{cases}$$

Proof. Let us denote $\rho' = (x_i - x_\mu^{b,l+1})\cos\phi + (y_i - y_\mu^{b,l+1})\sin\phi$ for a given i and $z' = z_i - z_\mu^{b,l+1}$. Then

$$\sum_{q=1}^{n^{l+1}} M_{qp}^l \int_0^{\chi_{\max}} u_q^{l+1}(\chi) K(\chi, z', \rho')\,\mathrm{d}\chi = \int \mathrm{d}\chi u_p^l(\chi) K(\chi, z, x\cos\phi + y\sin\phi) \times \sum_{q=1}^{n^{l+1}} (u_q^{l+1}(\chi))^* \int_0^{\chi_{\max}} u_q^{l+1}(\chi) K(\chi, z', \rho')\,\mathrm{d}\chi.$$

The proof would be straightforward if

$$K(\chi, z', \rho') \approx \sum_{q=1}^{n^{l+1}} (u_q^{l+1}(\chi))^* \int_0^{\chi_{\max}} u_q^{l+1}(\chi) K(\chi, z', \rho')\,\mathrm{d}\chi.$$

However, this is not true in general.

The following identity can be proved:

$$M_{pq}^l = \frac{s_p^{l+1}}{s_q^l} \int (v_q^l(z,\rho))^* v_p^{l+1}(z + z_{ab}, \rho + x_{ab}\cos\phi + y_{ab}\sin\phi)\,\mathrm{d}z\,\mathrm{d}\rho, \tag{12}$$

with $x_{ab} = x_\mu^{b,l+1} - x_\mu^{a,l}$, $y_{ab} = y_\mu^{b,l+1} - y_\mu^{a,l}$ and $z_{ab} = z_\mu^{b,l+1} - z_\mu^{a,l}$.

With this identity

$$\begin{aligned}\sum_{q=1}^{n^{l+1}} M_{qp}^l \int_0^{\chi_{\max}} u_q^{l+1}(\chi) K(\chi, z', \rho')\,\mathrm{d}\chi &\approx \frac{1}{s_p^l} \int_0^{\chi_{\max}} \mathrm{d}\chi \int \mathrm{d}z\,\mathrm{d}\rho (v_q^l(z,\rho))^* K(\chi, z, \rho) \\ &\quad \times K(\chi, z' + z_{ab}, \rho' + x_{ab}\cos\phi + y_{ab}\sin\phi) \\ &= \int_0^{\chi_{\max}} \mathrm{d}\chi u_q^l(\chi) K(\chi, z_i - z_\mu^{a,l}, (x_i - x_\mu^{a,l})\cos\phi + (y_i - y_\mu^{a,l})\sin\phi) \\ &= \mu_p^{a,l}(\phi).\end{aligned}$$

The error is bounded by the difference

$$\left| K(\chi, z + z_{ab}, \rho + x_{ab}\cos\phi + y_{ab}\sin\phi) - \sum_{q=1}^{n^{l+1}} s_q^{l+1} u_q^{l+1}(\chi) v_q^{l+1}(z + z_{ab}, \rho + x_{ab}\cos\phi + y_{ab}\sin\phi) \right| \leqslant \epsilon. \qquad \square$$

The bound ϵ/s_p^l means that for large p the coefficients are calculated less accurately than for small p. However, this does not affect the accuracy of the final result for the matrix vector product, since the potential at location r_j is obtained using:

$$\sum_p s_p^l v_p^l(z,\rho) \mu_p^{a,l}(\phi).$$

The error on the matrix vector product is therefore smaller than ϵ.

After applying Eq. (11), we are using an approximation to $\mu_p^{a,l}(\phi)$, $\tilde{\mu}_p^{a,l}(\phi)$, for which

$$\left| \mu_p^{a,l}(\phi) - \tilde{\mu}_p^{a,l}(\phi) \right| \leqslant \frac{\epsilon}{s_p^l}.$$

We prove that bound (11) remains valid when we use $\tilde{\mu}_p^{a,l}(\phi)$ instead of $\mu_p^{a,l}(\phi)$.

Proposition 7. *Assume that*

$$\left|\mu_q^{b,l+1}(\phi) - \tilde{\mu}_q^{b,l+1}(\phi)\right| \leqslant \frac{\epsilon}{s_q^{l+1}},$$

for all q, then

$$\left|\mu_p^{a,l}(\phi) - \sum_{q=1}^{n^{l+1}} M_{qp}^l(z, x\cos\phi + y\sin\phi)\tilde{\mu}_q^{b,l+1}(\phi)\right| \leqslant \frac{\epsilon}{s_p^l}.$$

This is essential to ensure the accuracy of the multilevel scheme.

Proof. Use Eq. (12).

Inner-to-Outer transform. Rokhlin and Yarvin [44] introduced a method of generalized Gaussian quadratures to integrate $K(\chi, z, \rho)$ over χ for a certain range of z and ρ. This quadrature can be used to compute $\mu_p^{a,l}(\phi)$ from $\lambda_p^{a,l}(\phi)$. This is done in the following way.

We start by computing

$$\sum_p \lambda_p^{a,l}(\phi) u_p^l(\chi).$$

This is an approximation of

$$\left|\sum_p \lambda_p^{a,l}(\phi) u_p^l(\chi) - \sum_i J_i K(\chi, z_i - z_\lambda^{a,l}, (x_i - x_\lambda^{a,l})\cos\phi + (y_i - y_\lambda^{a,l})\sin\phi)\right| \leqslant \epsilon.$$

We multiply by

$$K(\chi, z_\lambda^{a,l} - z_\mu^{b,l}, (x_\lambda^{a,l} - x_\mu^{b,l})\cos\phi + (y_\lambda^{a,l} - y_\mu^{b,l})\sin\phi) \stackrel{\text{def}}{=} T_{ba}^l(\chi, \phi). \qquad \square$$

We now prove that

Proposition 8. *The generalized Gaussian quadrature can be used to compute the integral over χ of:*

$$\mu_q^{a,l}(\phi) = \int u_q^l(\chi)\left\{\sum_b T_{ba}^l(\chi, \phi)\left(\sum_p \lambda_p^{a,l}(\phi) u_p^l(\chi)\right)\right\} \mathrm{d}\chi,$$

with accuracy ϵ/s_q^l.

Proof. Assume we are at level 0 and the size of the cluster is 1. Consider the following approximation based on an SVD:

$$\left|K(\chi, z, \rho) - \sum_{p=1}^{m} s_p u_p(\chi) v_p(z, \rho)\right| \leqslant \epsilon,$$

for any $\chi \in [0 : \chi_{\max}]$, $\chi_{\max} = \log 1/\epsilon$, $z \in [1 : 4]$ and $\rho \in [-4\sqrt{2} : 4\sqrt{2}]$.

Using this approximation, we construct a generalized Gaussian quadrature with $m/2$ points χ_k and weights ω_k. Consider two clusters C_a^0 and C_b^0 such that C_b^0 is in the interaction list of C_a^0, and two points $(x_i, y_i, z_i) \in C_a^0$ and $(x, y, z) \in C_b^0$. Then,

$$\left| \int K(\chi, z_i - z, (x_i - x)\cos\phi + (y_i - y)\sin\phi)\,\mathrm{d}\chi - \sum_{k=1}^{m/2} \omega_k K(\chi_k, z_i - z, (x_i - x)\cos\phi + (y_i - y)\sin\phi) \right| \leqslant \epsilon.$$

We have

$$\begin{aligned} K(\chi, z_i - z, (x_i - x)\cos\phi + (y_i - y)\sin\phi) = {} & K(\chi, z_\lambda^{b,0} - z, (x_\lambda^{b,0} - x)\cos\phi + (y_\lambda^{b,0} - y)\sin\phi) \\ & \times T_{ba}^0(\chi, \phi)\ K(\chi, z_i - z_\lambda^{a,0}, (x_i - x_\lambda^{a,0})\cos\phi \\ & + (y_i - y_\lambda^{a,0})\sin\phi). \end{aligned}$$

By applying the SVD to $K(\chi, z_\lambda^{b,0} - z, (x_\lambda^{b,0} - x)\cos\phi + (y_\lambda^{b,0} - y)\sin\phi)$ and using the fact that $v_p^0(z, \rho)$ is an orthonormal basis, we have proved that (χ_k, ω_k) can integrate

$$\int s_q^0 u_q^0(\chi) T_{ba}^0(\chi, \phi) K(\chi, z_i - z_\lambda^{a,0}, (x_i - x_\lambda^{a,0})\cos\phi + (y_i - y_\lambda^{a,0})\sin\phi)\,\mathrm{d}\chi,$$

with accuracy ϵ. Therefore, the error on $\mu_q^{b,0}(\phi)$ is of the order of ϵ/s_q^0. The same proof is applicable to any level l. □

5. Numerical tests

In will section, we will illustrate the stability for a wide frequency range of the method by some examples of our code. All results are obtained by an EFIE formulation without preconditioning.

For these tests, we have used $\mu_0 = 1.25751 \times 10^{-6}$, $\epsilon_0 = 8.84806 \times 10^{-12}$ giving $c = 299792548.2$ m/s; the objects are perfectly conductive.

The targeted error is 10^{-4} for the Kernel approximation, and the iterative solver (GMRES) stops when the residual becomes below than 10^{-4}.

5.1. Low-frequency regime: sphere $\lambda/15$

This example (Fig. 7) shows a radar cross-section (RCS) on the unit sphere of 3000 edges (dof) with a wavelength $\lambda = 30$. The exact solution is done by Mie Series.

This example has failed using the standard plane wave expansion (see Eq. (2)), even for three levels, the lowest number of levels for the FMM. This was due to numerical instabilities in the transfer functions $T_{p,\sigma}(r)$ (Eq. (3)).

The propagative term has been discretized with 4×7 points (variable σ) at level 3 and seven points for χ for the evanescent term.

5.2. Intermediate-frequency regime: sphere 2λ

This example (Fig. 8) shows a RCS on the unit sphere of 3000 edges with a wave length $\lambda = 1$. The exact solution is done by Mie Series.

The standard plane wave expansion has failed on this example when we are using more than five levels.

The propagative term has been discretized with 16×31 points (variable σ) at level 3, 10×19 at level 4, and with five and six points for χ for the evanescent term.

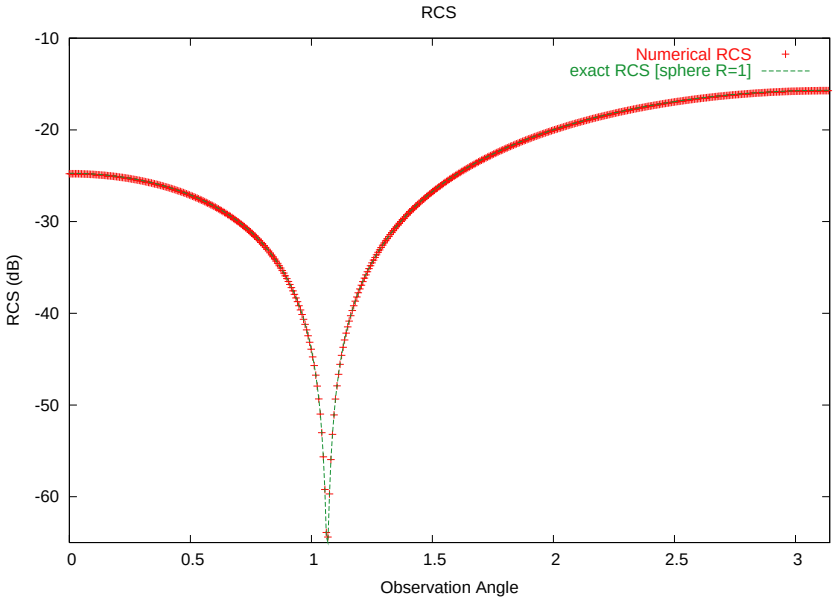

Fig. 7. RCS of the unit sphere of size $\lambda/15$.

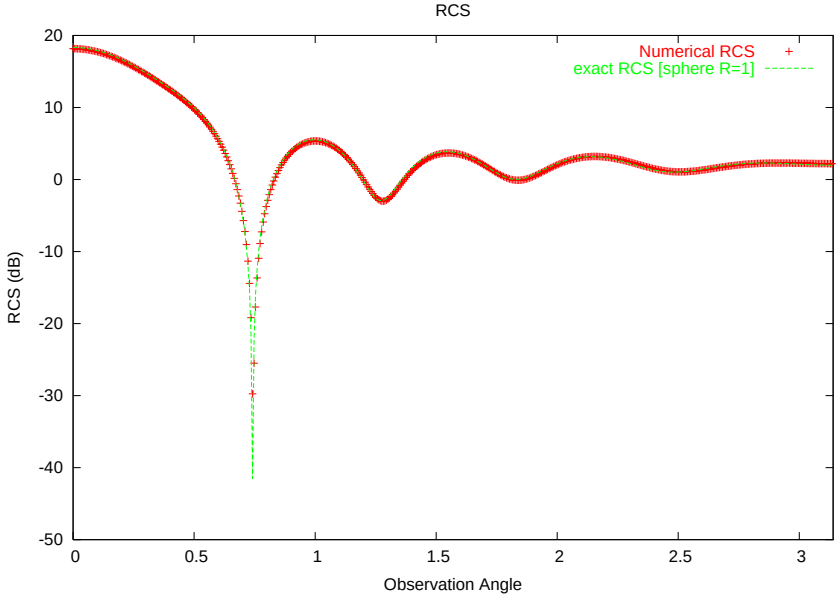

Fig. 8. RCS of unit sphere of size 2λ.

5.3. High-frequency regime: sphere 5.5λ

This example (Fig. 9) shows an RCS on unit sphere of 18,000 edges with a wave length $\lambda = 0.36$. The exact solution is done by Mie Series.

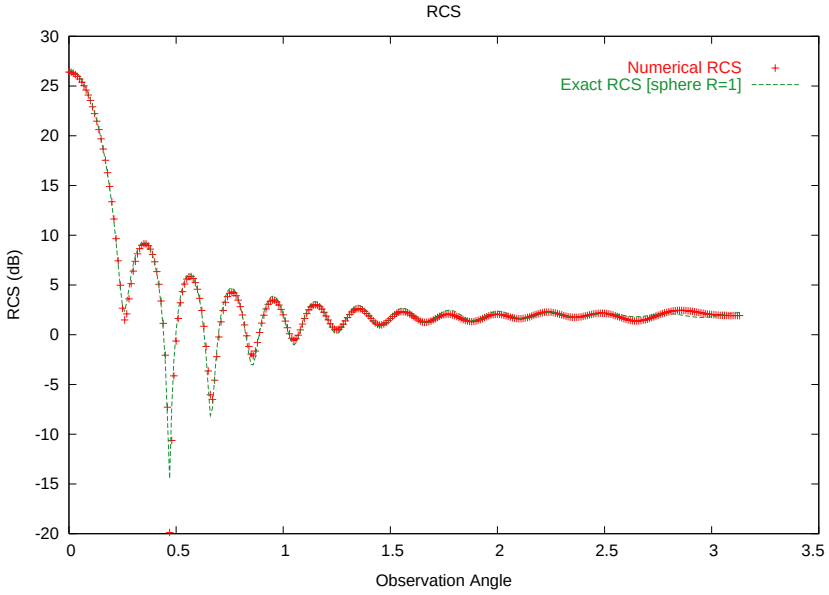

Fig. 9. RCS of unit sphere of size 5.5λ.

The propagative term has been discretized with 26×71 points at level 3, 20×39 points at level 4 and four points for χ for the evanescent term.

5.4. Comparison of the stable plane wave FMM and the low-frequency MLFMA

The stable plane wave FMM (SPW-FMM) and low-frequency MLFMA (LF-MLFMA) can both be used to solve low-frequency electromagnetic scattering. In this section, we compare their memory requirement and computational expense in a range of frequency from $\kappa = 10^{-4}$ to $\kappa = 10$.

Figs. 10 and 11 show the memory requirement, which is estimated using the size of the discretization for a single cluster of radius 1, i.e., the number of multipole coefficients. LF-MLFMA values are estimations based on the worst convergence case in Eq. (1). This worst case is given by the transfer vector $r = (2, 0, 0)$ and a local transfer vector $r' = (1, 1, 1)$. Those memory requirements appear to be very similar.

Regarding the computational cost, Figs. 12 and 13 show the benefit of our new expansion for the Inner-to-Outer step (the most expensive step in both methods). This cost is given as the number of floating point operations for one Inner-to-Outer step. LF-MLFMA values are $2(n_{\mathrm{FMA}})^2$ flops, where n_{FMA} is the discretization size. This corresponds to the cost of a matrix–vector product of size n_{FMA}. SPW-FMM values are $4n_{\mathrm{SPW}}$ flops, where n_{SPW} is the discretization size. This corresponds to the cost of a complex term-by-term product. SPW-FMM Inner-to-Outer cost is an order of magnitude below than LF-MLFMA for all frequencies.

5.5. Car $\lambda/2$

This example (Fig. 14) shows the electric intensity on the surface of a car of 18,000 edges with a wave length $\lambda = 30$.

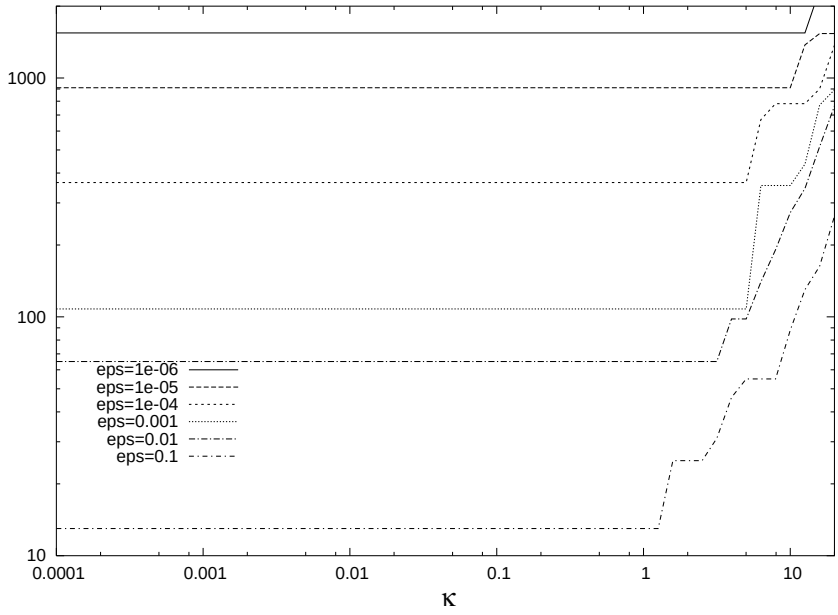

Fig. 10. Number of multipole coefficients for LF-MLFMA as a function of κ for various ϵ.

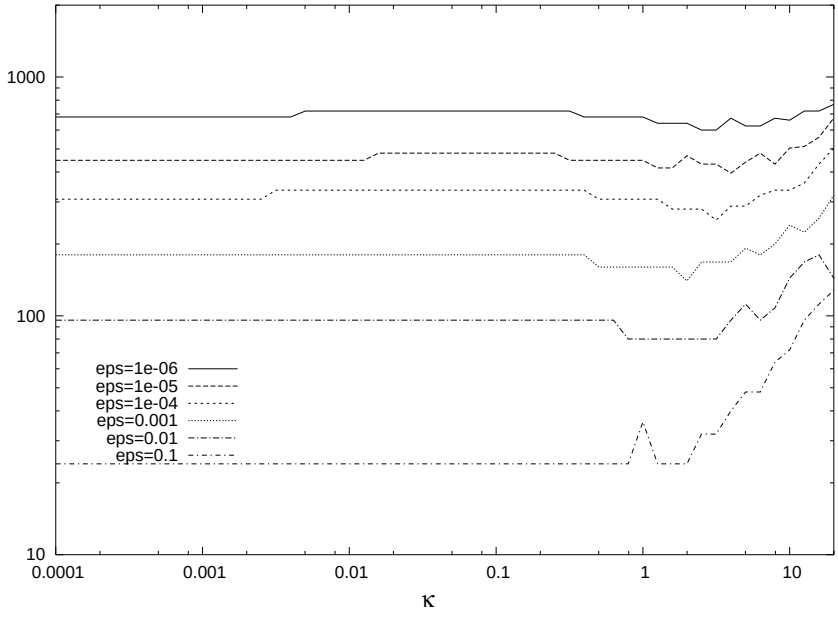

Fig. 11. Number of multipole coefficients for SPW-FMM as a function of κ for various ϵ.

The standard plane wave expansion has failed on this example when we are using more than three levels.

The propagative term has been discretized with 7×13 points at level 3, 5×9 points at level 4 and seven points for χ for the evanescent term.

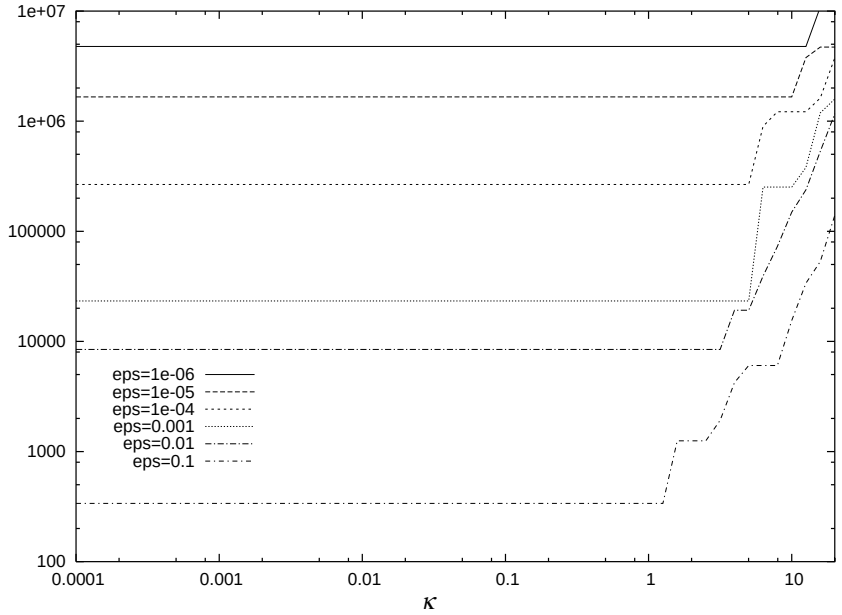

Fig. 12. Computational cost of the Inner-to-Outer step for LF-MLFMA as a function of κ for various ϵ.

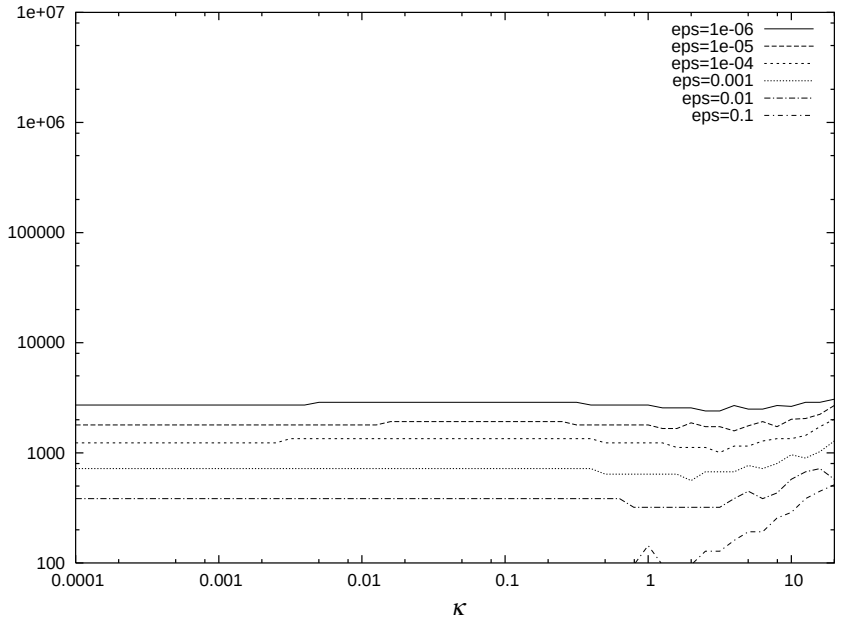

Fig. 13. Computational cost of the Inner-to-Outer step for SPW-FMM as a function of κ for various ϵ.

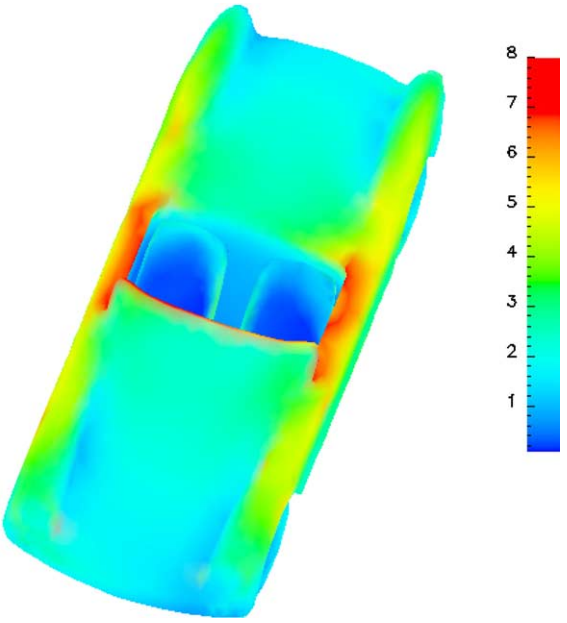

Fig. 14. Electric Intensity on the surface of a car.

6. Conclusion

The proposed method, SPW-FMM, allows to compute interactions with the kernel $\exp(\imath\kappa r)/r$ in the low and high-frequency regime. It is more stable and accurate than the standard plane wave expansion and has a lower computational cost than the classical fast multipole expansion.

Acknowledgements

The authors thank Prof. Olivier Pironneau, Prof. Parviz Moin, the Jacques-Louis Lions laboratory at Pierre et Marie Curie University and the Center for Turbulence Research at Stanford University, for their support.

References

[1] W.C. Chew, J.M. Jin, C.C. Lu, E. Michielssen, J.M.M. Song, Fast solution methods in electromagnetics, IEEE Trans. Antenn. Propag. 45 (3) (1997) 533–543.
[2] V. Rokhlin, Rapid solution of integral equations of classical potential theory, J. Comput. Phys. 60 (2) (1985) 187.
[3] N. Engheta, W. Murphy, V. Rokhlin, M.S. Vassiliou, The fast multipole method for (FMM) electromagnetic scattering problems, IEEE Trans. Antenn. Propag. 40 (6) (1992) 634–641.
[4] M.A. Epton, B. Dembart, Multipole translation theory for three-dimensional Laplace and Helmholtz equations, SIAM J. Sci. Comput. 16 (4) (1995) 865–897.
[5] B. Dembart, E. Yip, A 3D fast multipole method for electromagnetics with multiple levels, in: Proceedings of the 11th Annual Review of Progress in Applied Computational Electromagnetics, vol. 1, Monterey, CA, 1995, pp. 621–628.
[6] B. Dembart, G. Shubin, A 3D fast multipole method for electromagnetics with multiple levels, Technical document ISSTECH-97-004, Boeing, December 1994.

[7] B. Dembart, E. Yip, A 3-D moment method code based on fast multipole, in: URSI Radio Science Meeting Dig., Seattle, WA, 1994, p. 23.
[8] W. Elliott, J. Board, Fast Fourier-transform accelerated fast multipole algorithm, SIAM J. Sci. Comput. 17 (2) (1996) 398–415.
[9] L. Greengard, V. Rokhlin, A new version of the fast multipole method for the Laplace equation in three dimensions, Acta Numer. 229.
[10] C. White, M. Headgordon, Rotating around the quartic angular-momentum barrier in fast multipole method calculations, J. Chem. Phys. 105 (12) (1996) 5061–5067.
[11] J.-S. Zhao, W.C. Chew, Applying matrix rotation to the three-dimensional low-frequency multilevel fast multipole algorithm, Microw. Opt. Technol. Lett. 26 (2) (2000) 105–110.
[12] L. Greengard, J. Huang, V. Rokhlin, S. Wandzura, Accelerating fast multipole methods for low frequency scattering, IEEE Comput. Sci. Engrg. Mag.
[13] J.-S. Zhao, W.C. Chew, Three-dimensional multilevel fast multipole algorithm from static to electrodynamic, Microw. Opt. Technol. Lett. 26 (1) (2000) 43–48.
[14] J.-S. Zhao, W.C. Chew, MLFMA for solving integral equations of 2-D electromagnetic problems from static to electrodynamic, Microw. Opt. Technol. Lett. 20 (5) (1999) 306–311.
[15] J.-S. Zhao, W.C. Chew, Applying LF-MLFMA to solve complex PEC structures, Microw. Opt. Technol. Lett. 28 (3) (2001) 155–160.
[16] V. Rokhlin, Rapid solution of integral equations of scattering theory in two dimensions, J. Comput. Phys. 86 (2) (1990) 414–439.
[17] V. Rokhlin, Diagonal forms of translation operators for the Helmholtz equation in three dimensions, Research Report YALEU/DCS/RR-894, Department of Computer Science, Yale University, March 1992.
[18] C.C. Lu, W.C. Chew, A multilevel algorithm for solving boundary-value scattering, Microw. Opt. Technol. Lett. 7 (10) (1994) 466–470.
[19] J. Song, C.-C. Lu, W.C. Chew, Multilevel fast multipole algorithm for electromagnetic scattering by large complex objects, IEEE Trans. Antenn. Propag. 45 (10) (1997) 1488–1493.
[20] E. Darve, The fast multipole method (i): error analysis and asymptotic complexity, SIAM Numer. Anal. 38 (1) (2000) 98–128.
[21] E. Darve, The fast multipole method: numerical implementation, J. Comput. Phys. 160 (1) (2000) 195–240.
[22] W.C. Chew, Fast algorithms for wave scattering developed at the University of Illinois's electromagnetics laboratory, IEEE Antenn. Propag. Mag. 35 (4) (1993) 22–32.
[23] W.C. Chew, J. Jin, C.-C. Lu, E. Michielssen, J. Song, Fast solution methods in electromagnetics, IEEE Trans. Antenn. Propag. 45 (3) (1997) 533–543.
[24] J. Song, W.C. Chew, Multilevel fast-multipole algorithm for solving combined field integral equations of electromagnetic scattering, Microw. Opt. Technol. Lett. 10 (1) (1995) 14–19.
[25] W.C. Chew, C.-C. Lu, Y.M. Wang, Review of efficient computation of three-dimensional scattering of vector electromagnetic waves, J. Opt. Soc. Am. A 11 (1994) 1528–1537.
[26] C.C. Lu, W.C. Chew, Fast far-field approximation for calculating the RCS of large objects, Microw. Opt. Technol. Lett. 8 (5).
[27] J. Song, C.-C. Lu, W.C. Chew, S. Lee, Fast Illinois solver code (FISC) solves problems of unprecedented size at the center for computational electromagnetics, University of Illinois Technical Report CCEM-23-97, University of Illinois, Urbana Champaign, IL, 1997.
[28] J. Song, C. Lu, W.C. Chew, S. Lee, Fast Illinois solver code (FISC), IEEE Antenn. Propag. Mag. 40 (3) (1998) 27–33.
[29] C. Lu, W.C. Chew, A multilevel algorithm for solving a boundary integral equation of wave scattering, Microw. Opt. Technol. Lett. 7 (10) (1994) 466–470.
[30] R.L. Wagner, W.C. Chew, A ray-propagation fast multipole algorithm, Microw. Opt. Technol. Lett. 7 (10) (1994) 435–438.
[31] J. Song, W.C. Chew, Error analysis for the truncation of multipole expansion of vector Green's functions, IEEE Microw. Wireless Comp. Lett. 11 (7) (2001) 311–313.
[32] S. Koc, J. Song, W.C. Chew, Error analysis for the numerical evaluation of the diagonal forms of the scalar spherical addition theorem, SIAM J. Numer. Anal. 36 (3) (1999) 906–921.
[33] D. Solvason, H. Petersen, Error estimates for the fast multipole method, J. Statist. Phys. 86 (1–2) (1997) 391–420.
[34] S. Amini, A. Profit, Analysis of the truncation errors in the fast multipole method for scattering problems, J. Comput. Appl. Math. 115 (1–2) (2000) 23–33.
[35] B. Dembart, E. Yip, The accuracy of fast multipole methods for Maxwell's equations, IEEE Comput. Sci. Engrg. 5 (3) (1998) 48–56.
[36] S. Bindiganavale, J. Volakis, Guidelines for using the fast multipole method to calculate the RCS of large objects, Microw. Opt. Technol. Lett. 11 (4) (1996) 190–194.
[37] S. Ohnuki, W.C. Chew, A study of the error controllability of MLFMA, Antennas and Propagation Society, IEEE. Int. Symp. 3 (2001) 774–777.
[38] B. Hu, W.C. Chew, Fast inhomogeneous plane wave algorithm for multi-layered medium problems, in: IEEE Antennas and Propagation Society International Symposium, Transmitting Waves of Progress to the Next Millennium, Salt Lake City, UT, 2000, pp. 606–609.

[39] B. Hu, W.C. Chew, E. Michielssen, J. Zhao, Fast inhomogeneous plane wave algorithm (FIPWA) for the fast analysis of two-dimensional scattering problems, University of Illinois, Urbana.
[40] B. Hu, C. Chew, W.E. Michielssen, J. Zhao, Fast inhomogeneous plane wave algorithm for the fast analysis of two-dimensional scattering problems, Radio Sci. 34 (4) (1999) 759–772.
[41] B. Hu, W.C. Chew, Fast inhomogeneous plane wave algorithm for electromagnetic solutions in layered medium structures: two-dimensional case, Radio Sci. 35 (1) (2000) 31–43.
[42] B. Hu, C. Chew, W.S. Velamparambil, Fast inhomogeneous plane analysis of electromagnetic wave algorithm for the scattering, Radio Sci. 36 (6) (2001) 1327–1340.
[43] B. Hu, W.C. Chew, Fast inhomogeneous plane wave algorithm for scattering from objects above the multilayered medium, IEEE Trans. Geosci. Remote Sensing 39 (5) (2001) 1028–1038.
[44] N. Yarvin, V. Rokhlin, Generalized Gaussian quadratures and singular value decompositions of integral operators, Technical Report 1109, Department of Computer Science Research Report, Yale University, 1996.